Structure of human Aichi virus and implications for receptor binding

Ling Zhu[1,3$], Xiangxi Wang[2,$], Jingshan Ren[1], Abhay Kotecha[1], Thomas S. Walter[1], Shuai Yuan[2], Teruo Yamashita[4], Tobias J. Tuthill[3], Elizabeth E. Fry[1*], Zihe Rao[2,5*] and David I. Stuart[1,6*]

[1]Division of Structural Biology, University of Oxford, The Henry Wellcome Building for Genomic Medicine, Headington, Oxford OX3 7BN, UK. [2]National Laboratory of Macromolecules, Institute of Biophysics, Chinese Academy of Science, Beijing, 100101, China. [3]The Pirbright Institute, Pirbright, Surrey GU24 0NF, UK. [4]Deptartment of Microbiology and Medical Zoology, Aichi Prefectural Institute of Public Health, Aichi 4628576 Japan, [5]Laboratory of Structural Biology, School of Medicine, Tsinghua University, Beijing, 100084, China, [6]Diamond Light Source, Harwell Science and Innovation Campus, Didcot OX11 0DE, UK.

[$] These authors contributed equally to this work.

* Correspondence should be addressed to DIS (Email: dave@strubi.ox.ac.uk) or Z.R. (raozh@xtal.tsinghua.edu.cn) or EEF (liz@strubi.ox.ac.uk).

Aichi virus, an unusual and poorly characterized picornavirus can cause severe gastroenteritis in children. We have determined its three dimensional structure at 3.7 Å resolution, revealing a structure intermediate between the enteroviruses and cardioviruses, with a shallow, narrow depression bounded by the prominent VP0 CD loops (linking the C and D strands of the β-barrel), replacing the depression known as the 'canyon', frequently the site of receptor attachment in enteroviruses. VP0 is not cleaved to form VP2 and VP4 hence the 'VP2' β-barrel structure is complemented with a unique extended structure on the inside of the capsid. On the outer surface, a polyproline helix structure, not seen previously in picornaviruses is present at the C-terminus of VP1, a position where integrin binding motifs are found in some other picornaviruses. A peptide corresponding to this polyproline motif somewhat attenuates virus infectivity presumably blocking host cell attachment. This may guide cellular receptor identification.

The *Picornaviridae* is a family of small (300 Å diameter) icosahedral viruses with single-stranded positive sense RNA genomes, classified into many genera. Aichivirus (AiV) is a member of the Kobuvirus genus. High resolution structures are available for representative viruses from the *Enterovirus, Cardiovirus, Aphthovirus, Hepatovirus, Senecavirus* and *Parechovirus* genera[1], but until now not for any Kobuvirus. Aichi virus usually infects humans subclinically, but can lead to acute

gastroenteritis[2] and deaths in children below five years old especially in developing countries[3]. The seroprevalence of AiV is approximately 60% in children less than 10 years old and reaches 90% later in life[4,5]. Although AiV is considered as a potential global public health threat, there is no available vaccine or effective antiviral treatment.

AiV has limited sequence similarity with other picornaviruses (15-34% amino acid sequence identity), and it exhibits several distinctive features. Like parechoviruses, AiV capsids comprise VP0, VP1 and VP3. The extremely long VP0 (370 residues) does not undergo the final, maturation cleavage to VP2 and VP4 which is assumed to be RNA catalyzed. It remains unclear whether VP0 is myristoylated, despite having the classic myristoylation motif (GXXXT) at the N terminus[6]. The AiV genome has an unusually high C content and reportedly the highest degree of RNA secondary structure in picornaviruses[7]. Unlike most picornaviruses, both the non-structural proteins L and 2A of AiV have neither a protease nor an autocatalytic motif, but are involved in viral RNA replication and encapsidation[6,8,9]. Furthermore, AiV is the sole picornavirus identified to contain an RNA encapsidation signal at the 5′–terminal RNA stem loop[10]. Finally the AiV capsid proteins possess an unusually high proline content.

We have analyzed AiV genotype A864/88 strain (Methods). Sucrose density gradient

purification yielded a band, at the density expected for picornaviruses (1.25–1.30 g cm^{-3}), comprising mature viruses containing packaged RNA (**Supplementary Fig. 1**). The presence of only 3 capsid proteins, VP0, VP1 and VP3 was confirmed by SDS PAGE (**Supplementary Fig. 1**). Negative stain electron microscopy showed mature viruses with morphology indistinguishable from other picornaviruses (**Supplementary Fig. 1**).

We imaged purified AiV using cryo-EM with a Gatan K2 Summit detector (see Methods, **Supplementary Fig. 2**). A total of 25,279 particles were subjected to three-dimensional reconstruction and a 'gold standard' resolution of 3.68 Å (Fourier Shell correlation (FSC) =0.143) was achieved. The map was of sufficient quality to allow the atomic modeling of most capsid proteins (Methods and **Fig. 1**). The model was refined and validated using standard X-ray crystallographic methods[11] (**Table 1 and Table 2**).

The AiV capsid is well ordered, apart from a number of disordered residues in VP0 (80-114) and VP1 (254-278). The capsid proteins (VP0, VP1 and VP3) adopt the classical eight-stranded anti-parallel β-barrel configuration and follow the expected pseudo T = 3 symmetry (where T is the triangulation number), such that VP1 surrounds the 5-fold axes and VP0 and VP3 alternate about the 2- and 3-fold axes (**Fig. 2 and Supplementary Fig. 3**). The AiV structure reveals the presence of

capsid pores similar to those seen in foot-and-mouth disease virus (FMDV, aphthovirus genus) at the 5-fold axes, which are thought to be permeable to ions such as Caesium[12]. A structure-based phylogenetic tree constructed from the biological protomers of picornaviruses and picorna-like insect viruses indicates that AiV lies almost equidistant from the entero, cardio, aphtho, and hepato genera, being slightly closer to the enteros and cardios (**Fig. 2b**). The external surface of AiV lacks the marked protrusion from the icosahedral 5-fold axes of Ljungan virus (LV, genus parechovirus), and is less angular than that of Hepatitis A virus (HAV, genus hepatovirus) (**Fig. 2a**). Nevertheless in contrast to FMDV where short surface loops produce a rather smooth surface, the loops at the 5-fold and 3-fold axes in AiV are slightly longer and raised, giving the virus "cooling tower" structures around the 5-fold axes (**Fig. 2a**). AiV possesses some surface depressions analogous to those referred to as the "canyon" (a continuous depression surrounding the five-fold axes of symmetry) and "pit" (discrete depressions in the same region), which form the site of receptor binding in many picornaviruses[13-15] (**Fig. 2c**). Compared to HAV, the VP1 BC loop of AiV is extended to build the north wall of the canyon while the movement of the VP1 GH loop (part of the south wall) narrows the front part of the depression. A long insertion in the VP0 CD loop partly compensates for the reduction in the VP0 EF loop to form the back part of the depression, which is broader and flatter (**Fig. 2c**).

Overall AiV VP1 most closely resembles that from aphthoviruses and cardioviruses than from other picornaviruses with an r.m.s. deviation of ~2.8-3.0 Å for ~80-85% matched Cαs for these five viruses based on a comparison of 15 known structures (**Supplementary Fig. 4**). AiV VP1 has a unique 'puff" structure connecting the αA helix and βB strand, which is absent in other picornaviruses (**Supplementary Fig. 3**). In-line with AiV's similarity to the aphtho- and cardioviruses, it does not contain the hydrophobic pocket seen in the enteroviruses where expulsion of a lipidic moiety is a pre-requisite for uncoating[13,16]. In AiV, compared to enteroviruses the VP1 β-barrel is compressed, a shift in the βC strand and reorganization of the CD loop directly block the entrance to the pocket, and the remaining space is filled by large side chains (**Fig. 2d**). The VP1 BC, EF and GH loops, important antigenic sites in other picornaviruses[15], vary in length and fold in AiV (**Supplementary Fig 5**). The overall fold of AiV VP3 is similar to other picornaviruses, (**Supplementary Fig. 4**), but it does not bear the N-terminal A/LRM (arginine/lysine-rich motif), which mediates RNA attachment in parechoviruses[17]. This might reflect differences in the mechanism of genome encapsidation.

At 370 residues AiV VP0 is the longest of known picornaviruses, and there is no reported cleavage of VP0 into VP2 and VP4 in the genus *Kobuvirus*. Sequence and structural comparisons show that the VP0 core domain (VP2 counterpart) is most similar to VP2 in Mengovirus (RMSD for 83% of Cαs is 1.9 Å) (**Supplementary**

Fig. 4), however the VP0 N-terminal domain (VP4 counterpart) exhibits little similarity to other VP4s (**Fig. 2e** and **Supplementary Fig. 6**). AiV does not possess the VP2 N-terminal domain swap configuration observed in HAV, LV and insect picorna-like viruses across the 2-fold axis, where it enhances interactions with the neighboring pentamers[17,18]. An approximately 30 residue insertion in the CD loop of the AiV VP0 core domain (residues 195-253), is strikingly exposed on the external surface, forming the south wall of the depression, leaving an extremely short βC strand (**Fig. 2c** and **Supplementary Fig. 3**), this CD loop might play a role in receptor binding and we propose this to be an epitope of significant antigenicity. The VP0 N-terminal domain (predicted to be 113 residues in length based on the structural alignment of AiV VP0 with VP2 of other picornaviruses) is ~30-50 residues longer than VP4s in other picornaviruses. There is a disordered region (residues 80-114) which may interact with the RNA genome. VP4 or its equivalent is the most diverse of the picornavirus capsid proteins, varying in length, location and conformation between genera (**Fig. 2e** and **Supplementary Fig. 6**). Notably, the long VP4 counterpart in AiV folds back on itself forming a "bow and arrow" shape and has a greater number of interactions with other protomers in a pentamer. As in other picornaviruses the N-termini of the capsid proteins form an extensive network at the inner surface, which links 5-fold related protomers together to form pentamers.

Determination of the stability of virus particles is critical for decontamination and to

guide vaccine design. The 2-fold interaction mediated by the VP2 αA helices, which separate during the initial stages of enterovirus uncoating[13,16], play key roles in the stability of particles[19]. The separation of the VP2 αA helices at the icosahedral 2-fold of AiV is 5.3Å compared to HAV-3.8 Å, EV71-7.3 Å, polio-7.6 Å and FMDV-8.2 Å (**Fig. 3a**), presenting a relatively tight packing. Despite this relatively tight packing AiV displayed the stability of a typical enterovirus and became unstable at lower pH (**Fig. 3b, 3c**). The low fluorescence signals at low temperature using SYTO9 dye to detect RNA exposure implies that even at pH 4 AiV does not expose its RNA at room temperature. To correlate particle stability with the structure, we systematically analyzed the interactions between any one subunit and its environment within the protomer, within the pentamer and between pentamers by PISA[20] (**Supplementary Table 1**). Together with our previous results, FMDV (O serotype), AiV, EV71, CVA16, LV and HAV release their genomes under neutral pH at 50°C, 55°C, 58°C, 59°C, 61°C and 68°C respectively by heat-treatment[16,18,19,21,22]. We found that the interactions between pentamers determine the particle stability with a compelling correlation of 0.923 (**Fig. 3d**). This supports the proposal that enhancing the interactions between pentamers would be a target for the rational design of picornavirus vaccines with improved stability[19].

Although receptors have been identified for many picornaviruses[23-25], the receptor for AiV remains unknown. Certain picornaviruses possess an

168 arginine-glycine-aspartic acid (RGD) or KGD motif at the C-terminus of VP1 which
169 is involved in integrin recognition[26,27]. Whilst this is not present in AiV there is
170 instead, a proline-rich fragment with sequence P_{228}XPPPPXPPXPXP$_{240}$ at this same
171 position, presenting an extended poly-L-proline type II (PPII) helix, on the external
172 surface of AiV (**Fig. 4a** and **Fig. 4b**). As noted AiV has an unusually high proline
173 content and there are two other PPII helices in the capsid (residue 50-63 in VP0 and
174 residue 228-240 in VP1), however the VP1 C-terminal helix is the longest. Likely
175 due to their peculiar propensity to be solvent-exposed, PPII helices are frequently
176 involved in protein-protein interactions in signal transduction, antigen recognition,
177 cell-to-cell communication and viral pathogenesis[28,29]). This PPII helix might serve
178 as a recognition signal for cellular receptor(s) or virulence factors to manipulate the
179 host's cellular machinery[29]. Such a PPII helix is unprecedented in picornaviruses,
180 although they are observed in other viruses. A prototypical example is represented by
181 the HIV-1 Nef, which necessarily functions through protein-protein interaction by its
182 polyproline segment (P_{69}VRPQVPLRP$_{78}$) for full pathogenicity of the virus[30]. To
183 understand if there might be a role for this structure in cell attachment we
184 investigated if a peptide version of the helix might inhibit infection. The results (**Fig.**
185 **4c**) do indeed show a partial inhibition, in particular, pre-attachment of peptides to
186 cells was able to inhibit by nearly 50% infection of Aichi virus, suggesting that this
187 structure is capable of partially competing with the virus.
188

In summary AiV exhibits a number of distinctive features and seems to occupy an evolutionary position between the enteroviruses and other picornaviruses, using an uncoating mechanism yet to be determined but different to that of enteroviruses. Furthermore we suggest that a highly exposed polyproline helix at the C-terminus of VP1 is a recognition motif for binding to the enteric receptor. This would imply a mode of engagement with the host cell unlike others described for picornaviruses.

METHODS

Virus production and purification

The AiV stock was strain A846/88, GenBank: BAA31356.1. The virus was amplified using 40 x 175 cm^2 flasks of Vero cells innoculated at a multiplicity of infection (MOI) of 1. Vero cells were cultured in Dulbecco's modified Eagle's medium (DMEM; Sigma-Aldrich) supplemented with 1% fetal bovine serum (FBS; Gibco) and grown at 37°C in a humidified atmosphere containing 5% CO2. After 90% of cells showed CPE, the flasks were frozen and thawed three times, and the cultures centrifuged to remove cell debris. The supernatant was centrifuged for 3 h at 95,000 g and virus pellets resuspended in PBST buffer (phosphate-buffered saline containing 0.01% Triton X-100), then loaded onto 15-45% (w/v) sucrose density gradients and centrifuged at 222,000 g for 4 h in a SW41 rotor at 4 °C. The lower band was pooled and subjected to 35-55% (w/w) discontinuous sucrose gradient centrifugation at 28,000 rpm for 20 h.

211

212 **Negative stain electron microscopy**

213 Purified AiV was concentrated to ~0.3 mg/mL and applied onto glow-discharged,
214 Formvar/carbon-coated copper grids (Electron Microscopy Sciences). After 60
215 seconds incubation, excess sample was blotted away and the grids washed twice with
216 deionized water. Samples were stained with 1% (w/v) uranyl acetate for 60 s and
217 excess stain removed. We examined the grids on a Tecnai T12 (FEI, Hillsboro, OR)
218 transmission electron microscope operated at 80kV. Images were taken using a 4k x 4k
219 high-sensitivity FEI Eagle camera (FEI, Hillsboro, OR) at a nominal magnification of
220 67,000×.

221

222 **Cryo-EM and data collection**

223 A 3 µL aliquot of purified AiV virions (~3 mg/mL) was deposited onto freshly
224 glow-discharged 400-mesh holey carbon-coated copper grids (C-flat, CF-2/1-2C,;
225 Protochips Inc.) followed by 3 s blotting in 70% relative humidity for
226 plunge-freezing (Vitrobot; FEI, Hilsboro, OR) in liquid ethane. Images were
227 acquired with a Tecnai G2 Polara microscope (FEI, Hillsboro, OR) fitted with a K2
228 Summit direct electron detector (Gatan, Abingdon, UK) operating at 300 kV high
229 tension voltage. Micrographs were collected at defocuses between 1.6 and 3 µm as
230 movies (25 frames, each 0.2 s, giving a total dose of 25 e^{-} $Å^{-2}$) in single electron
231 counting mode using SerialEM at a calibrated magnification of 37,027×, resulting in

232 a pixel size of 1.35 Å.

233

234 **Image processing and 3D reconstruction**

235 Frames 3-22 were used and corrected for beam-induced drift by aligning and
236 averaging the individual frames of each movie using MOTIONCORR[31]. Particles
237 were picked automatically by ETHAN[32] and false-positives manually removed using
238 the boxer program in EMAN[33]. Gctf[34] was used to estimate the CTF parameters for
239 drift corrected micrographs and micrographs with significant astigmatism or drift
240 were discarded. A total of 25,279 particles from 776 micrographs were picked for the
241 2D alignment and 3D reconstruction using Relion 1.3[35] using recommended
242 gold-standard refinement procedures and applying icosahedral symmetry I4. The
243 initial model for AiV was generated by low-pass filtering the reconstructed HAV
244 structure to 30 Å. We conducted two rounds of 2D classification and 3D refinement
245 to further select the particles for final refinement. The final resolution was evaluated
246 using the "gold standard" Fourier shell correction (threshold = 0.143 criterion)[36,37].
247 The dataset and refinement statistics are summarized in **Table. 1**.

248

249 **Model building, refinement and structure analysis**

250 The atomic models of AiV capsid proteins VP0, VP1 and VP3 were manually built
251 into the density map with the structures of ERAV capsid proteins as a guide in
252 COOT[38]. Amino acid registration was accomplished solely based on the clear

densities for "landmark" stretches of residues. REFMAC[39] was used to calculate difference maps to highlight errors in the model. These full-atom models were further improved in a pseudo-crystallographic manner by iterative positional and B-factor refinement in real space using Phenix[11] and rebuilt in COOT[38], against the Relion map. This procedure was used only to improve atomic models, not to modify the 3.7 Å cryo-EM density map. Densities for individual proteins were segmented, put in artificial crystal lattices, and then used to calculate their structural factors. The amplitudes and phases of these structural factors were used as pseudo-experimental diffraction data for model refinement in Phenix[11]. The quality of the final model was confirmed visually by analyzing the match between map densities and coordinates and by the calculation of correlation coefficients and R-factors with REFMAC[39]. Refinement statistics are given in **Table 2** as evaluated by Molprobity[40] functions integrated in Phenix[11]. Structure-based phylogenetic trees were constructed as described by Riffel et al[41].

Inhibition of AiV infection in Vero cells by VP1 C-terminal peptide

For pre-attachment assays, peptide (P_{228}XPPPPXPPXPXP$_{240}$) at concentrations ranging from 5 nM to 50 μM was incubated with AiV at a multiplicity of infection (MOI) of 0.5 or with Vero cells at 37 °C for 1h, then the virus-peptide mixtures were added into Vero cells or the cells incubated with peptides were inoculated with AiV at MOI of 0.5 and using AiV without peptides as a control. For the post-attachment

assay, Vero cells were infected with AiV at MOI of 0.5 at 37 °C for 1h and peptide at varying concentrations was subsequently added. Cells exposed to concentrations of peptide ranging from 5 nM to 50 μM alone were used to evaluate the cytotoxicity. Cells were cultured in DMEM supplemented with 1% FBS and grown at 37 ˚C with 5% CO_2. At 48h post infection (p.i.), cells were observed to evaluate the appearance of CPE.

Thermal stability assay

PaSTRy[42] experiments were performed using a MX3005p RT-PCR instrument (Agilent) employing both SYTO9 and SYPRO-Red (Invitrogen) dyes to detect the presence of RNA and the exposed hydrophobic regions of proteins respectively. 50 μL reactions were set up in a thin-walled PCR plate (Agilent), containing ~1 μg of the Aichi virus, 5 mM SYTO9 (excitation 492 nm, emission 517 nm) and 3 × SYPRO-Red (excitation 535 nm, emission 665 nm) in PBS (pH 7.4), and the temperature ramped from 25 to 99 ˚C in 1 ˚C intervals with fluorescence recorded in triplicate, always at 25 ˚C. This results in an expanding saw-tooth temperature profile which reduces the self-quenching effect of temperature on the dyes.

Accession code: The atomic coordinates of Aichivirus has been submitted to the Protein Data Bank with accession number PDB: XXX. The cryo-EM density map of Aichivirus has been deposited with the Electron Microscopy Data Bank:

EMD-XXX.

Supplementary Information is available in the online version of the paper.

Acknowledgements

We thank Jun Dong and Jonathan Diprose for IT support and the OPIC electron microscopy facility for microscope provision and Kai Zhang for data processing. Work was supported by the Ministry of Science and Technology 973 Project (grant nos. 2014CB542800), National Science Foundation grant no. 31570717 and 81520108019, the Strategic Priority Research Program of the Chinese Academy of Sciences, grant no. XDB08020200 and the MRC grants G100099 and MR/N00065X/1. The work of the Wellcome Trust Centre in Oxford is supported by the Wellcome Trust core award 090532/Z/07/Z. The OPIC electron microscopy facility was founded by a Wellcome Trust JIF award (060208/Z/00/Z) and is supported by a WT equipment grant (093305/Z/10/Z). The Wellcome Trust, MRC and BBSRC also supports the National EM facility, which enabled provision of the K2 detector. The Pirbright Institute receives strategic funding from the BBSRC. J.R. is Wellcome Trust-supported, EEF and DIS are supported by the MRC (grant no G100099), and D.I.S. is supported as a Jenner Investigator.

Author Contributions L.Z., X.W., T.S.W and T.Y, prepared samples, L.Z., X.W., Y.S, A.K., J.R., T.J.T and T.S.W. assisted in research. X.W., E.E.F, T.J.T and D.I.S.

316 designed the study, all authors analysed data and X.W., L.Z., J.R., E.E.F., Z.R. and
317 D.I.S. wrote the manuscript.

318

319

Table 1

Cryo-EM imaging and data processing statistics.

Statistics	AiV
Micrographs (total)	776
Micrographs (used)	668
Particles selected	25,279
Particles included in final reconstruction	18,566
Sampling, Å per pixel	1.35
Defocus range, μm	1.5-3.0
Resolution, Å	3.68
(gold standard FSC = 0.143 criterion)	

Table 2

Model refinement statistics.

Statistics	AiV
Rmsd (bond angles, °)	1.5
Rmsd (bond lengths, Å)	0.010
Ramachandran statistics	
Most favoured (%)	90.7
Allowed	8.0
Outliers	1.3
Rwork/Rfree* (%)	32.6/32.9

*Rfree was calculated for 5% of reflections randomly excluded from the refinement

330

331 **Figures**

332 **Figure 1** | The 3.68 Å resolution (overall) cryo-EM structure of Aichi. **(a)** Cryo-EM
333 image of AiV. **(b)** The gold-standard FSC curves of the final maps with a resolution
334 of 3.68 Å at FSC=0.143. **(c)** and **(d)** The final AiV map was analyzed by ResMap
335 showing resolution distribution from 2.9 to 4.4 Å. Most of the capsid has a
336 resolution of better than 3.0 Å, the resolution of the interior parts of the map
337 (corresponding to RNA genome) is ~8-30 Å. Electron density map for a protomeric
338 unit of AiV capsids **(e)**, VP1, VP0 and VP3 are colored in blue, green and red
339 respectively. **(f)** Sections of VP1, VP0 and VP3.

340

341 **Figure 2** | Overall structures, phylogeny and structural features. **(a)** Comparison of
342 capsids from AiV with LV, HAV, FMDV and Enterovirus 71 (EV71). The capsids are
343 coloured by radius from blue to red according to the scale bar shown. **(b)**
344 Structure-based evolutionary relationship among viruses from *Picornaviridae*
345 (circled by dashed lines) and *Dicistroviridae* (circled by solid line): CVB3,
346 coxsackievirus B3; PV1, poliovirus type 1; HRV14, human rhinovirus 14; BEV1,
347 bovine enterovirus type 1; EV71, EV-A71; TMEV, Theilers virus; MEV, Mengo
348 virus; SVV, Seneca valley virus; FMDV, foot-and-mouth disease virus; ERAV,
349 equine rhinitis A virus; HAV, hepatitis A virus; AiV, Aichi virus; TrV, triatoma virus;
350 CrPV, cricket paralysis virus. **(c)** Surface of the biological protomer of AiV,
351 poliovirus and HAV. Loops forming the canyon walls in poliovirus are drawn thicker,

the CD loop constituting the "pit" in AiV is also labeled. **(d)** Close up view of pocket. βC strand (left) and βH strand for EV71 (orange, pocket factor magenta), HRV14 (yellow), FMDV (blue) and AiV (green) are presented in ribbon format. Bulky side chains shown as sticks occlude the AiV and FMDV pockets. **(e)** The unique structure of VP0 N-terminus (VP4 counterpart) in AiV shown in cartoon representation, whilst the remaining structure is rendered as a surface. A pentamer of icosahedral protomeric units is shown, the colouring scheme uses the signature colours (VP1 blue, VP2 counterpart green and VP3 red). The view is from the inside of the virus.

Figure 3 | Particle stability and the correlation between particle stability and interaction areas. **(a)** The separation of VP2 α-helices at the icosahedral two fold of HAV (green, 3.8 Å), AiV (blue, 5.3 Å), EV71 (sky blue, 7.3 Å), Polio (grey, 7.6 Å), FMDV (orange, 8.2 Å) and 80S-like EV71 (red, 12.2 Å). (**b, c**) The thermal stability of AiV. The stability of AiV across the pH range from 4.0 to 9.5 was determined by scanning fluorimetry assay PaSTRy using the dye SYTO9 to detect RNA exposure. (**b**) The raw fluorescence traces of AiV incubated with SYTO9; their first derivatives are shown in (**c**). The colour scheme is red (pH 4.0), orange (pH 5.0), yellow (pH 6.0), green (pH 7.0), sky blue (pH 8.0), blue (pH 9.0) and purple (pH 9.5). (**d**) Correlation plot of interaction areas between pentamers versus experimental particle stability. Particle stability for representative viruses was characterized experimentally at pH 7.0.

373

374 **Figure 4** | A proline-rich motif, a potential receptor binding site in AiV. (**a**) Location
375 of proline-rich motifs on the external surface of the AiV pentamer. The colour
376 scheme is the same as **Fig. 2e**, the proline-rich motifs are highlighted in blue. (**b**)
377 Side view of a proline-rich motif at the C-terminus of VP1. (**c**) Peptides of the
378 proline-rich motif in VP1 decrease AiV infection in Vero cells at 48h. The inhibitory
379 ability of the peptides was detected by cytopathic effects (CPE) when cells were
380 exposed to the peptides before or after the virus was allowed to infect cells. The
381 result showed that high concentrations of peptide exhibited a partial inhibition, in
382 particular pre-attachment of peptides to cells nearly halved AiV inhibition.. All data
383 were obtained in triplicate.

384

385

References

1. King, A.M., Adams, M.J. & Lefkowitz, E.J. *Virus taxonomy: classification and nomenclature of viruses: Ninth Report of the International Committee on Taxonomy of Viruses*, (Elsevier, 2011).
2. Reuter, G., Boros, Á. & Pankovics, P. Kobuviruses–a comprehensive review. *Reviews in medical virology* **21**, 32-41 (2011).
3. Richman, D.D., Whitley, R.J. & Hayden, F.G. *Clinical virology*, (American Society for Microbiology Press, 2009).
4. Sdiri-Loulizi, K. et al. Aichi virus IgG seroprevalence in Tunisia parallels genomic detection and clinical presentation in children with gastroenteritis. *Clinical and Vaccine Immunology* **17**, 1111-1116 (2010).
5. Ribes, J.M., Montava, R., Téllez-Castillo, C.J., Fernández-Jiménez, M. & Buesa, J. Seroprevalence of Aichi virus in a Spanish population from 2007 to 2008. *Clinical and Vaccine Immunology* **17**, 545-549 (2010).
6. Sasaki, J., Nagashima, S. & Taniguchi, K. Aichi virus leader protein is involved in viral RNA replication and encapsidation. *Journal of virology* **77**, 10799-10807 (2003).
7. Lukashev, A.N. et al. Genetic variation and recombination in Aichi virus. *Journal of general virology* **93**, 1226-1235 (2012).
8. Sun, Y. et al. An open conformation determined by a structural switch for 2A protease from coxsackievirus A16. *Protein & cell* **4**, 782-792 (2013).
9. Sasaki, J. & Taniguchi, K. Aichi virus 2A protein is involved in viral RNA replication. *Journal of virology* **82**, 9765-9769 (2008).
10. Sasaki, J. & Taniguchi, K. The 5′-end sequence of the genome of Aichi virus, a picornavirus, contains an element critical for viral RNA encapsidation. *Journal of virology* **77**, 3542-3548 (2003).
11. Afonine, P.V. et al. Towards automated crystallographic structure refinement with phenix. refine. *Acta Crystallographica Section D: Biological Crystallography* **68**, 352-367 (2012).
12. Acharya, R. et al. The three-dimensional structure of foot-and-mouth disease virus at 2.9 Å resolution. (1989).
13. Dang, M. et al. Molecular mechanism of SCARB2-mediated attachment and uncoating of EV71. *Protein & cell* **5**, 692-703 (2014).
14. Tuthill, T.J., Groppelli, E., Hogle, J.M. & Rowlands, D.J. Picornaviruses. in *Cell Entry by Non-Enveloped Viruses* 43-89 (Springer, 2010).
15. Wang, X. et al. A sensor-adaptor mechanism for enterovirus uncoating from structures of EV71. *Nature structural & molecular biology* **19**, 424-429 (2012).
16. Ren, J. et al. Picornavirus uncoating intermediate captured in atomic detail. *Nature communications* **4**(2013).
17. Zhu, L. et al. Structure of Ljungan virus provides insight into genome packaging of this picornavirus. *Nature communications* **6**(2015).
18. Wang, X. et al. Hepatitis A virus and the origins of picornaviruses. *nature* (2014).
19. Kotecha, A. et al. Structure-based energetics of protein interfaces guides foot-and-mouth

disease virus vaccine design. *Nature structural & molecular biology* **22**, 788-794 (2015).

20. Krissinel, E. & Henrick, K. Inference of macromolecular assemblies from crystalline state. *Journal of molecular biology* **372**, 774-797 (2007).
21. De Colibus, L. et al. More-powerful virus inhibitors from structure-based analysis of HEV71 capsid-binding molecules. *Nature structural & molecular biology* (2014).
22. Ren, J. et al. Structures of coxsackievirus A16 capsids with native antigenicity: implications for particle expansion, receptor binding, and immunogenicity. *Journal of virology* **89**, 10500-10511 (2015).
23. Jackson, T., Sheppard, D., Denyer, M., Blakemore, W. & King, A.M. The epithelial integrin αvβ6 is a receptor for foot-and-mouth disease virus. *Journal of virology* **74**, 4949-4956 (2000).
24. Mendelsohn, C.L., Wimmer, E. & Racaniello, V.R. Cellular receptor for poliovirus: molecular cloning, nucleotide sequence, and expression of a new member of the immunoglobulin superfamily. *Cell* **56**, 855-865 (1989).
25. Yuan, S. et al. TIM-1 acts a dual-attachment receptor for Ebolavirus by interacting directly with viral GP and the PS on the viral envelope. *Protein & cell* **6**, 814-824 (2015).
26. Baranowski, E. et al. Cell recognition by foot-and-mouth disease virus that lacks the RGD integrin-binding motif: flexibility in aphthovirus receptor usage. *Journal of virology* **74**, 1641-1647 (2000).
27. Williams, Ç.H. et al. Integrin αvβ6 is an RGD-dependent receptor for coxsackievirus A9. *Journal of virology* **78**, 6967-6973 (2004).
28. Adzhubei, A.A., Sternberg, M.J. & Makarov, A.A. Polyproline-II helix in proteins: structure and function. *Journal of molecular biology* **425**, 2100-2132 (2013).
29. Berisio, R. & Vitagliano, L. Polyproline and triple helix motifs in host-pathogen recognition. *Current protein & peptide science* **13**, 855 (2012).
30. Vermeire, J., Vanbillemont, G., Witkowski, W. & Verhasselt, B. The Nef-infectivity enigma: mechanisms of enhanced lentiviral infection. *Current HIV research* **9**, 474-489 (2011).
31. Li, X. et al. Electron counting and beam-induced motion correction enable near-atomic-resolution single-particle cryo-EM. *Nature methods* **10**, 584-590 (2013).
32. Kivioja, T., Ravantti, J., Verkhovsky, A., Ukkonen, E. & Bamford, D. Local average intensity-based method for identifying spherical particles in electron micrographs. *Journal of structural biology* **131**, 126-134 (2000).
33. Ludtke, S.J., Baldwin, P.R. & Chiu, W. EMAN: semiautomated software for high-resolution single-particle reconstructions. *Journal of structural biology* **128**, 82-97 (1999).
34. Zhang, K. Gctf: real-time CTF determination and correction. *Journal of structural biology* (2015).
35. Scheres, S.H. RELION: implementation of a Bayesian approach to cryo-EM structure determination. *Journal of structural biology* **180**, 519-530 (2012).
36. Scheres, S.H. & Chen, S. Prevention of overfitting in cryo-EM structure determination. *Nature methods* **9**, 853-854 (2012).
37. Henderson, R. et al. Outcome of the first electron microscopy validation task force meeting. *Structure* **20**, 205-214 (2012).

38. Emsley, P. & Cowtan, K. Coot: model-building tools for molecular graphics. *Acta Crystallographica Section D: Biological Crystallography* **60**, 2126-2132 (2004).
39. Brown, A. et al. Tools for macromolecular model building and refinement into electron cryo-microscopy reconstructions. *Acta Crystallographica Section D-Structural Biology* **71**, 136-153 (2015).
40. Chen, V.B. et al. MolProbity: all-atom structure validation for macromolecular crystallography. *Acta Crystallographica Section D: Biological Crystallography* **66**, 12-21 (2009).
41. Riffel, N. et al. Atomic resolution structure of Moloney murine leukemia virus matrix protein and its relationship to other retroviral matrix proteins. *Structure* **10**, 1627-36 (2002).
42. Walter, T.S. et al. A plate-based high-throughput assay for virus stability and vaccine formulation. *Journal of virological methods* (2012).

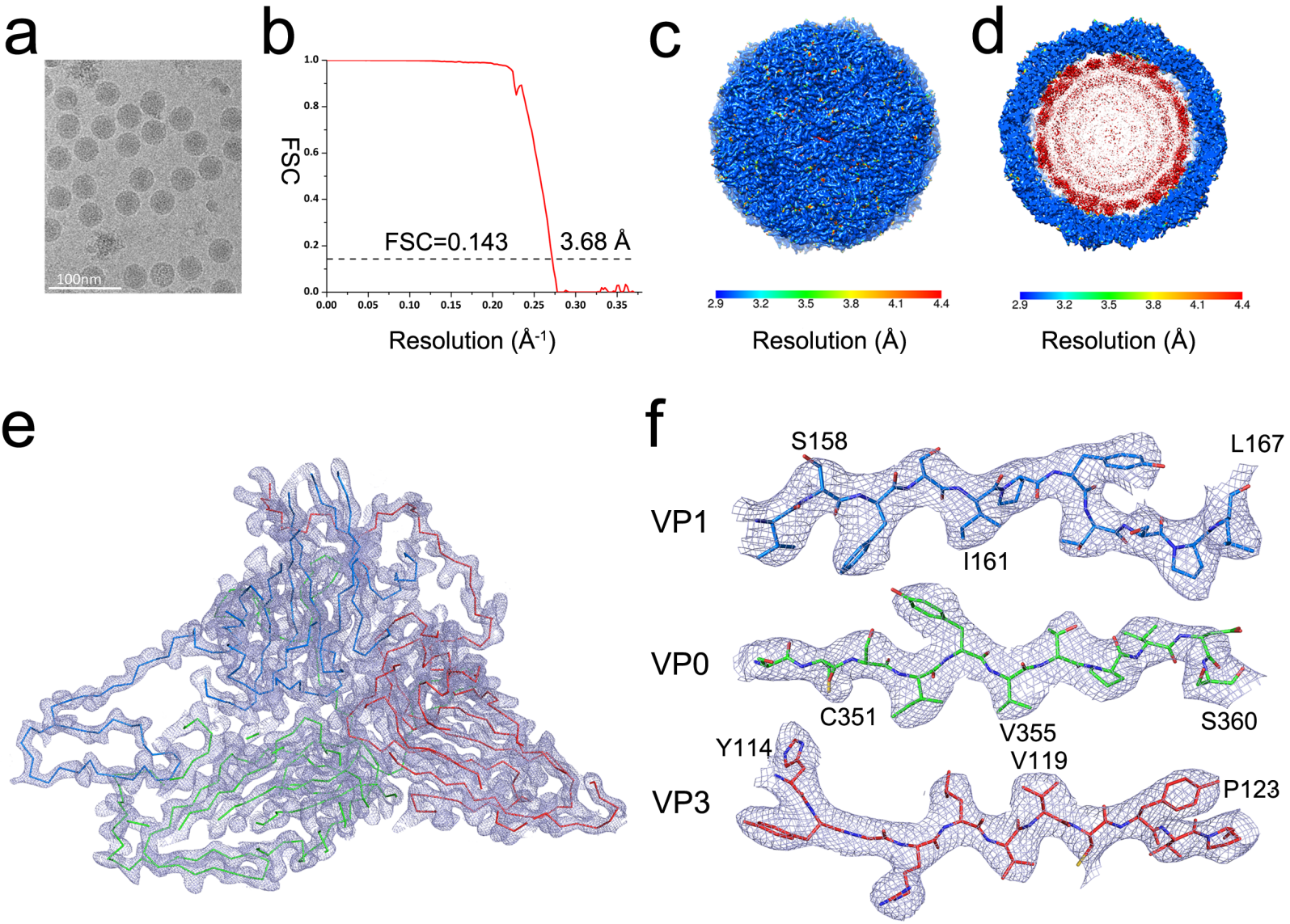
a
100nm
b
FSC
1.0
0.8
0.6
0.4
0.2
0.0
0.00
0.05
0.10
0.15
0.20
0.25
0.30
0.35
FSC=0.143
3.68 Å
Resolution (Å-1)
c
2.9
3.2
3.5
3.8
4.1
4.4
Resolution (Å)
d
2.9
3.2
3.5
3.8
4.1
4.4
Resolution (Å)
e
f
VP1
S158
L167
I161
VP0
C351
V355
S360
VP3
Y114
V119
P123

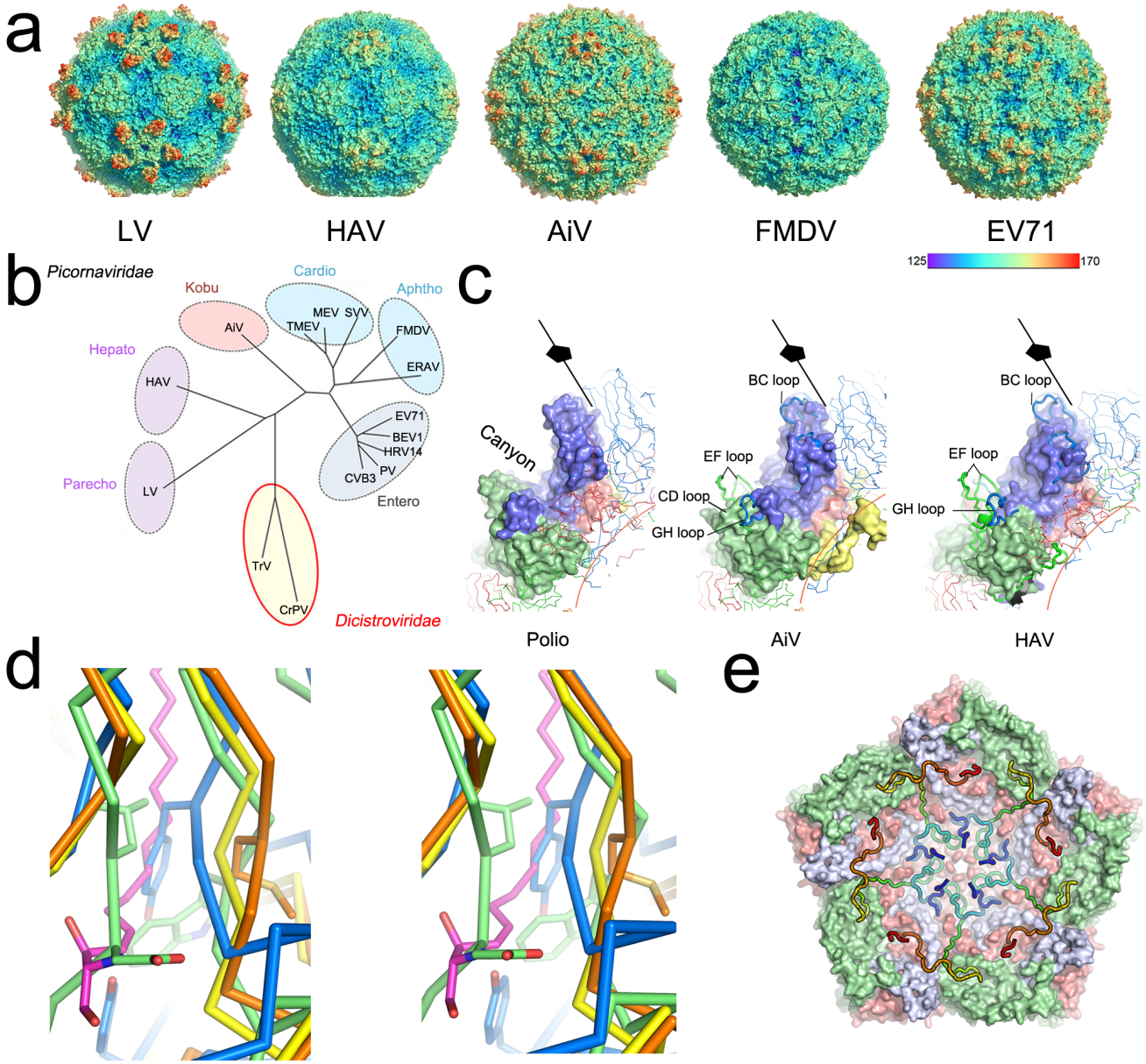
a
LV
HAV
AiV
FMDV
EV71
b
Picornaviridae
Kobu
Cardio
Aphtho
AiV
MEV
SVV
TMEV
FMDV
ERAV
Hepato
HAV
EV71
BEV1
HRV14
CVB3
PV
Parecho
LV
Entero
TrV
CrPV
Dicistroviridae
c
125
170
Canyon
BC loop
EF loop
CD loop
GH loop
Polio
AiV
HAV
d
e

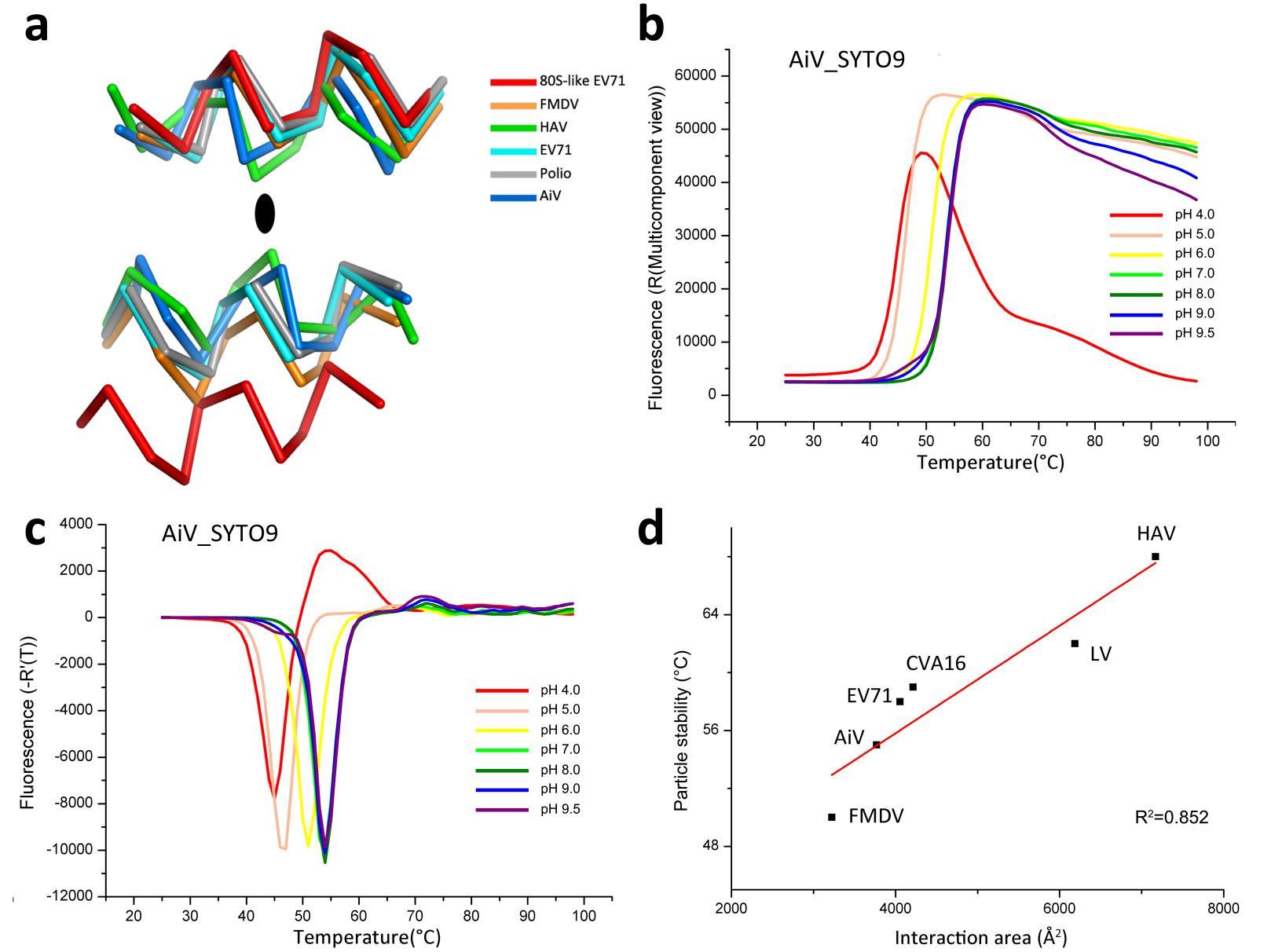
a
80S-like EV71
FMDV
HAV
EV71
Polio
AiV
b
AiV_SYTO9
Fluorescence (R(Multicomponent view))
Temperature(°C)
pH 4.0
pH 5.0
pH 6.0
pH 7.0
pH 8.0
pH 9.0
pH 9.5
c
AiV_SYTO9
Fluorescence (-R'(T))
Temperature(°C)
d
Particle stability (°C)
Interaction area (Å²)
HAV
LV
CVA16
EV71
AiV
FMDV
R²=0.852

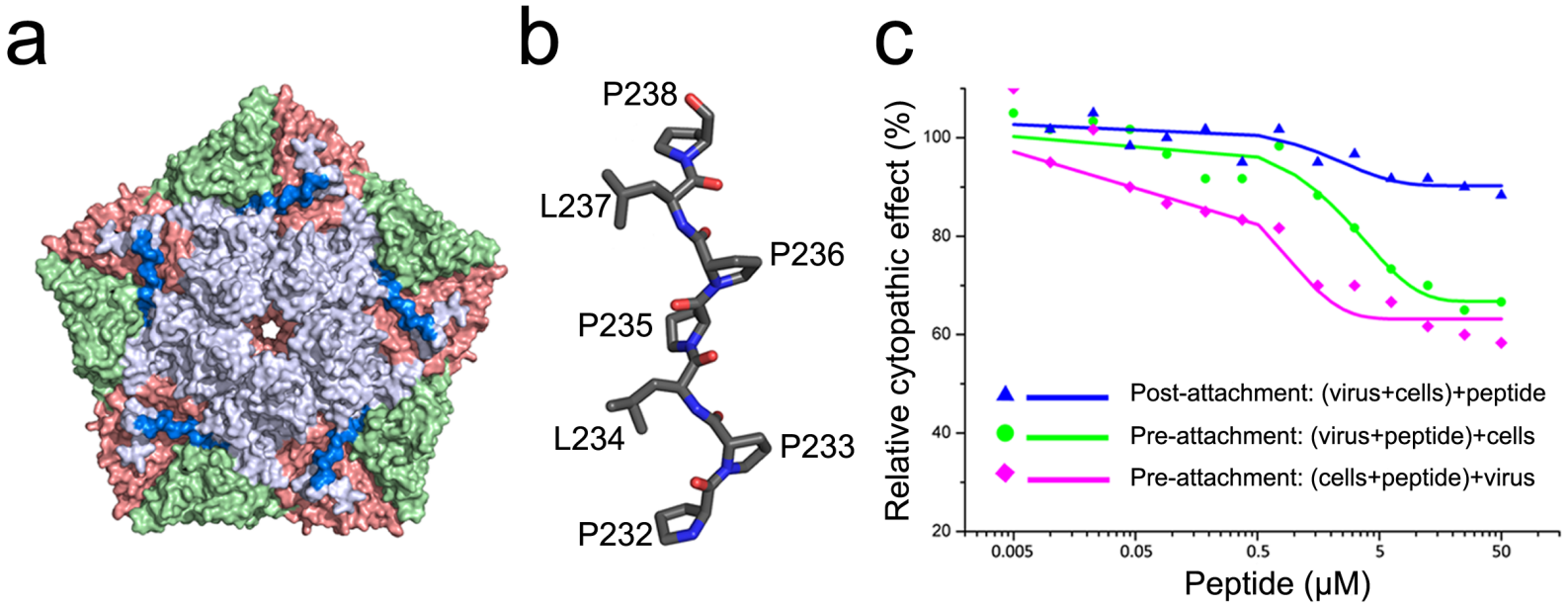
a
b
P238
L237
P236
P235
L234
P233
P232
c
Relative cytopathic effect (%)
100
80
60
40
20
0.005
0.05
0.5
5
50
Peptide (μM)
Post-attachment: (virus+cells)+peptide
Pre-attachment: (virus+peptide)+cells
Pre-attachment: (cells+peptide)+virus